Nanoscale mapping of the W/Si(001) Schottky barrier

Chris A. Durcan, Robert Balsano, and Vincent P. LaBella[a)]
College of Nanoscale Science and Engineering, State University of New York, Albany, New York 12203, USA

(Received 6 June 2014; accepted 28 June 2014; published online 10 July 2014)

The W/Si(001) Schottky barrier was spatially mapped with nanoscale resolution using ballistic electron emission microscopy (BEEM) and ballistic hole emission microscopy (BHEM) using *n*-type and *p*-type silicon substrates. The formation of an interfacial tungsten silicide is observed utilizing transmission electron microscopy and Rutherford backscattering spectrometry. The BEEM and BHEM spectra are fit utilizing a linearization method based on the power law BEEM model using the Prietsch Ludeke fitting exponent. The aggregate of the Schottky barrier heights from *n*-type (0.71 eV) and *p*-type (0.47 eV) silicon agrees with the silicon band gap at 80 K. Spatially resolved maps of the Schottky barrier are generated from grids of 7225 spectra taken over a 1 μm × 1 μm area and provide insight into its homogeneity. Histograms of the barrier heights have a Gaussian component consistent with an interface dipole model and show deviations that are localized in the spatial maps and are attributed to compositional fluctuations, nanoscale defects, and foreign materials. © *2014 AIP Publishing LLC*. [http://dx.doi.org/10.1063/1.4889851]

I. INTRODUCTION

When an interface is formed between a metal and semiconductor, charge is exchanged between the materials until the two Fermi energies equilibrate, creating a potential barrier called a Schottky barrier.[1,2] Schottky diodes have a low capacitance and recovery time and are also being studied as they are found in source drain contacts in silicon based MOSFETs.[3–7] For an *n*-type semiconductor to metal interface, the potential barrier formed is the energy difference between the Fermi level of the metal and the bottom of the conduction band in the semiconductor. For a *p*-type semiconductor to metal interface, the potential barrier formed is the energy difference between the Fermi level of the metal and the top of the valance band in the semiconductor. Theoretically, this barrier height is a function of the electron affinity in the semiconductor, the work function in the metal, and an interface dipole term which accounts for the rearrangement of the charge density due to the truncation of the bulk crystals and any interface bonding that may occur.[8] In this model, the aggregate of the Schottky barriers of an *n*-type and *p*-type metal to semiconductor junction should equal the band gap of the semiconductor.[9] The interface dipole term is naturally inhomogeneous for non-epitaxial interfaces and should result in a Gaussian like distribution of barrier heights.[10,11] In addition to interface dipoles, other effects, such as defects, foreign species, and compositional fluctuations, can also affect the spatial distribution of the Schottky barrier height on the nanometer length scale.[12–15]

Powerful techniques to probe metal to semiconductor interfaces with nanoscale precision are ballistic electron emission microscopy (BEEM) and ballistic hole emission microscopy (BHEM).[16] BEEM and BHEM have been used to measure the Schottky barrier height of many different metals to semiconductor interfaces.[17–34] BEEM and BHEM are three terminal scanning tunneling microscopy (STM) techniques; hot electrons (BEEM) or holes (BHEM) are injected into a grounded metal film and travel ballistically towards the interface. Electrons (or holes) which have enough forward momentum after traveling through the metal to surmount the Schottky barrier pass into the semiconductor and are collected as the BEEM (or BHEM) current. This unique method of injecting hot carriers through an STM tip allows for nanoscale spatial resolution in the measurement of carrier transmission at the interface. The energy diagrams for BEEM and BHEM are displayed in Figs. 3(a) and 3(c), respectively. In addition, BEEM and BHEM probes interface under zero-biased conditions, measuring the interface without changing the band structure, giving it high energetic resolution (~0.02 eV).[35]

When performing BEEM or BHEM measurements, either a series of spectra or a topographical map can be taken. When taking a spectrum, BEEM current is collected as a function of tip bias at a single location. When taking a topographical map, the STM tip moves across the surface, generating two images, simultaneously measuring the topography and the BEEM current for a given bias.[36,37] Spatially mapping the Schottky barrier is performed by recording BEEM current as a function of tip bias and location then fitting the spectra at each tip location to obtain the barrier height. Palm *et al*. mapped the Schottky barrier height of Au/Si(001) by taking 12 BEEM images while varying the tunnelling voltage from 0.5 V to 1.2 V. The BEEM current for each pixel was fit to the BEEM model to extract the Schottky barrier height, generating a spatial map.[38] A few studies have spatially mapped Schottky barrier heights by taking BEEM spectra. Fowell *et al*. measured the Schottky barrier of the Au/CdTe interface and showed spatial fluctuations in the Schottky barrier by acquiring 15 spectra over an image area of 40 nm × 20 nm.[39,40] Olbrich *et al*. measured the Schottky barrier height of a Au-Co film on GaAs over an area of 114 nm × 114 nm collecting 16 384 spectra. Cobalt grains encapsulated by gold demonstrated how the Schottky barrier spatially varies between two metals, showing two

[a)]Electronic address: vlabella@albany.edu

Gaussian like distributions, one for cobalt and the other for gold.[41] However, very little BEEM work has been preformed for the tungsten silicon interface.

In this article, the W/Si(001) Schottky barrier is measured and spatially mapped using BEEM and BHEM. This study consisted of grids of 7225 spectra over a 1 μm × 1 μm region taken on a W/Si(001) interface to study the Schottky barrier. A thin interfacial tungsten silicide is found to form utilizing transmission electron microscopy energy dispersive x-ray spectroscopy (TEM-EDX) and Rutherford backscattering spectrometry (RBS). When fit using the simplified BEEM model and using the Prietsch Ludeke (PL) fitting exponent, the *n*-type and *p*-type Schottky barriers sum to be bandgap of silicon. Histograms follow the general trend of a Gaussian distribution and show asymmetries which are attributed to compositional fluctuations in the silicide and nanoscale defects at the interface. The spatial Schottky barrier maps show that the majority of the area has a Schottky barrier near the mean of the histograms and appear to show some grouping. There are also localized spots (~20 nm^2) of higher Schottky barrier heights attributed to defects or foreign materials.

II. EXPERIMENTAL

The tungsten Schottky diodes were fabricated in a high-vacuum chamber using high resistivity *n*-type and *p*-type Si(001) by depositing tungsten on lightly doped Si(001). The single crystal silicon wafers had a resistivity of 100 Ω cm (phosphorus doped) and 10 Ω cm (boron doped), for *n*-type and *p*-type doping, respectively. The native oxide layer was removed utilizing a standard chemical hydrofluoric acid treatment immediately prior to loading into a high vacuum (10^{-8} mbar) deposition chamber.[24,29] The tungsten films were deposited onto the silicon using electron beam evaporation through a 2 mm by 2 mm shadow mask. The deposited metal thickness of all samples was 5 nm of tungsten with a 10 nm gold capping layer to inhibit tungsten oxide formation. Deposition thicknesses were calibrated using RBS and TEM-EDX in a JEOL Titan. After deposition, the samples were mounted onto a custom designed sample holder for BEEM and BHEM measurements. The plate allowed for simultaneous grounding of the metal film using a BeCu contact and connection of the silicon to an *ex situ* pico-ammeter to measure the BEEM and BHEM current. An ohmic contact was established by cold pressing indium onto the backside of the silicon substrate.

A modified low temperature STM (Omicron) was utilized for all BEEM and BHEM measurements at a pressure in the 10^{-11} mbar range.[42] The samples were inserted into the UHV chamber and loaded onto the STM stage and cooled to 80 K for all measurements. Two-point current-voltage measurements were taken *in situ* for each sample at low temperatures using a Keithley 2400 source measurement unit to verify rectifying behavior. All measurements were taken in the absence of ambient light. Pt/Ir STM tips, mechanically cut at a steep angle, were utilized for all BEEM and BHEM measurements. The experiment is shown schematically in the inset of Fig. 3 along with energy band diagrams. BEEM and BHEM spectra were acquired for *n*-type and *p*-type silicon; all measurements used a constant tunneling current setpoint of 20 nA with forward tip biasing, i.e., the carriers injected into the metal are the majority carriers in the semiconductor.

Spectra were taken every 11.7 nm throughout a 1 μm × 1 μm area of the metal surface, resulting in each sample accumulating 7225 spectra. All samples were introduced into a UHV environment within 3 h of metal deposition; the samples were cooled down to ~80 K immediately thereafter. The spectra were averaged into a single representative spectrum for each sample, as shown by Figs. 3(b) and 3(d). Both the averaged and all the individual spectrum were fit to the simplified form of the BEEM model $I_B \propto (V_t - \phi_b)^n$, where I_B is the BEEM current, ϕ_b is the Schottky barrier, V_t is the tip bias, and n is a fitting exponent of 5/2, given by the PL fitting model.[36] The fits were performed by linearizing the spectra and using standard linear regression, which returned the Schottky barrier and corresponding R^2 value, indicating the quality of the fit. The fits to the individual spectra were utilized to generate the Schottky barrier maps and histograms.

III. RESULTS

A TEM cross section and EDX line spectrum of the fabricated diode on *n*-type silicon is shown in Fig. 1, where the mass percent of gold, tungsten, silicon, and oxygen was measured. The EDX results show five distinct layers and the chemical species present in each band. The top layer is comprised entirely of gold, a second layer shows an intermixing of gold with tungsten, and a third layer shows a layer comprised entirely of tungsten. The two bottom layers consist of the underlying silicon substrate and an intermediate layer where tungsten and silicon intermix. The EDX shows no

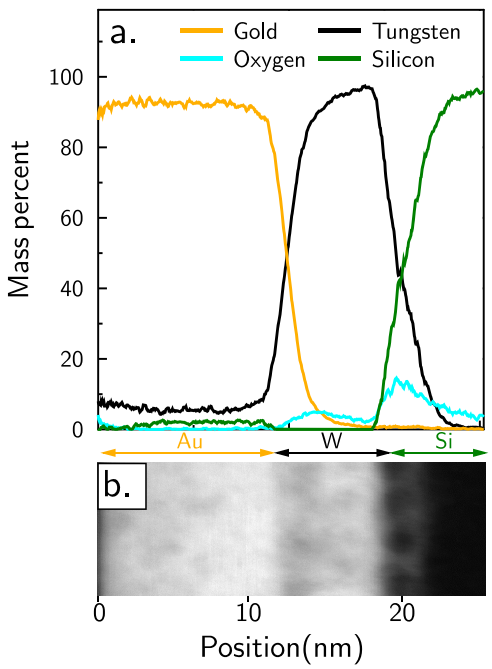

FIG. 1. (a) TEM-EDX scan of tungsten silicon Schottky barrier and (b) Cross section TEM image of EDX scan.

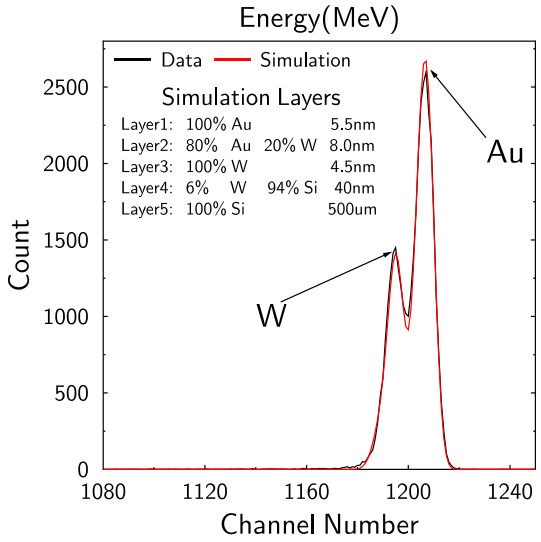

FIG. 2. The RBS (in black) and RUMP simulation (in red) of the tungsten silicon Schottky junction.

gold at the tungsten to silicon junction. The TEM image is the real space scan of the same region that EDX was performed on and shows five distinct bands as indicated. The RBS results and fit utilizing the RUMP software package are displayed in Fig. 2. The best possible fit shows five distinct layers, consistent with the EDX and TEM results.

The averaged BEEM and BHEM spectra are shown in Figs. 3(b) and 3(d), respectively. The tip bias starts at an energy below the Schottky barrier, and no BEEM (or BHEM) current is collected. As the tip bias increases, there is an increase in the current where the energy of the injected carriers has enough forward momentum to overcome the Schottky barrier. The averaged spectra taken from tungsten on *n*-type silicon sample are shown in Fig. 3(b). A tip bias less than 0.7 V results in no BEEM current, while a tip bias greater than 0.7 V results in the collection of BEEM current. Similarly, the averaged spectra taken from tungsten on *p*-type silicon are shown in Fig. 3(d). A tip bias greater than −0.5 V results in no BHEM current, while a tip bias less than −0.5 V results in the collection of BHEM current.

The linearized spectra and fits for the *n*-type and *p*-type silicon substrates are displayed in Figs. 4(a) and 4(c), respectively. The corresponding non-linearized spectra and fits for the *n*-type and *p*-type silicon substrates are displayed in Figs. 4(b) and 4(d), respectively. For the *n*-type silicon, the Schottky barrier height is 0.71 eV and for the *p*-type silicon, the Schottky barrier height is 0.47 eV, both fits have $R^2 > 0.999$. The sum of the absolute value of these two Schottky barriers heights is 1.18 eV.

For the *n*-type silicon substrate, a histogram of the barrier heights is displayed in Fig. 5(a). The histogram plots the Schottky barrier height of all of the spectra (94.2%) that could be fit with an average R^2 value of 0.93. The average Schottky barrier and standard deviation of the distribution are utilized to draw a Gaussian as a line over the histogram. The dotted vertical line is the Schottky barrier height determined from the fit to the average spectra, displayed in

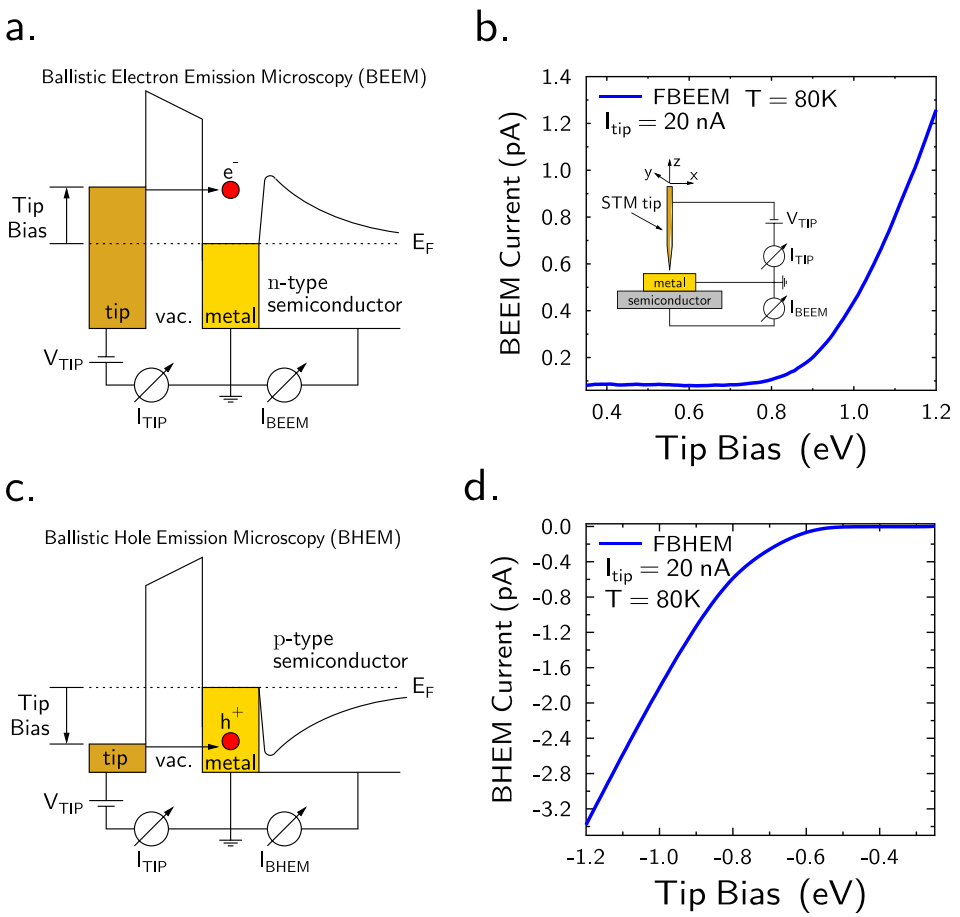

FIG. 3. (a) BEEM energy diagram. (b) Averaged BEEM spectra with inset showing schematic BEEM setup. (c) BHEM energy diagram. (d) Averaged BHEM spectra.

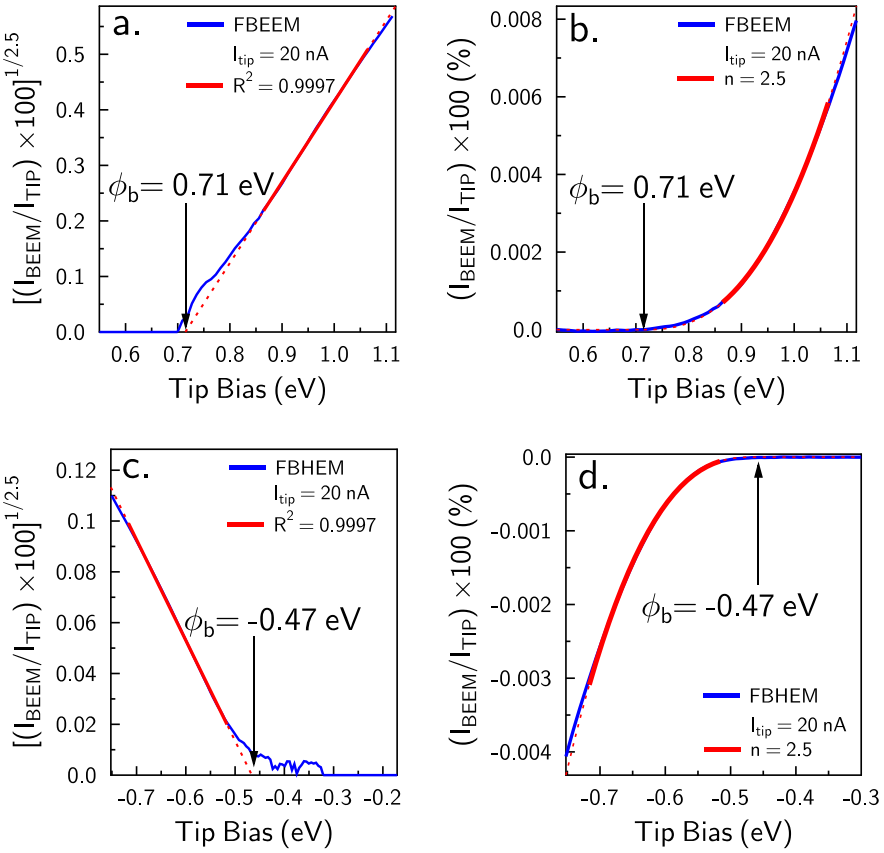

FIG. 4. (a) Linearized tungsten *n*-type silicon Schottky junction BEEM spectra and fit using exponent $n = 2.5$. Solid red line is fit and dotted red line is the extrapolated region fit to zero transmission. (b) Non linearized BEEM spectra and fit shown in (a). (c) Linearized tungsten *p*-type silicon Schottky junction BHEM spectra and fit using exponent $n = 2.5$. Solid red line is fit and dotted red line is the extrapolated region fit to zero transmission. (d) Non linearized BHEM spectra and fit shown in (c).

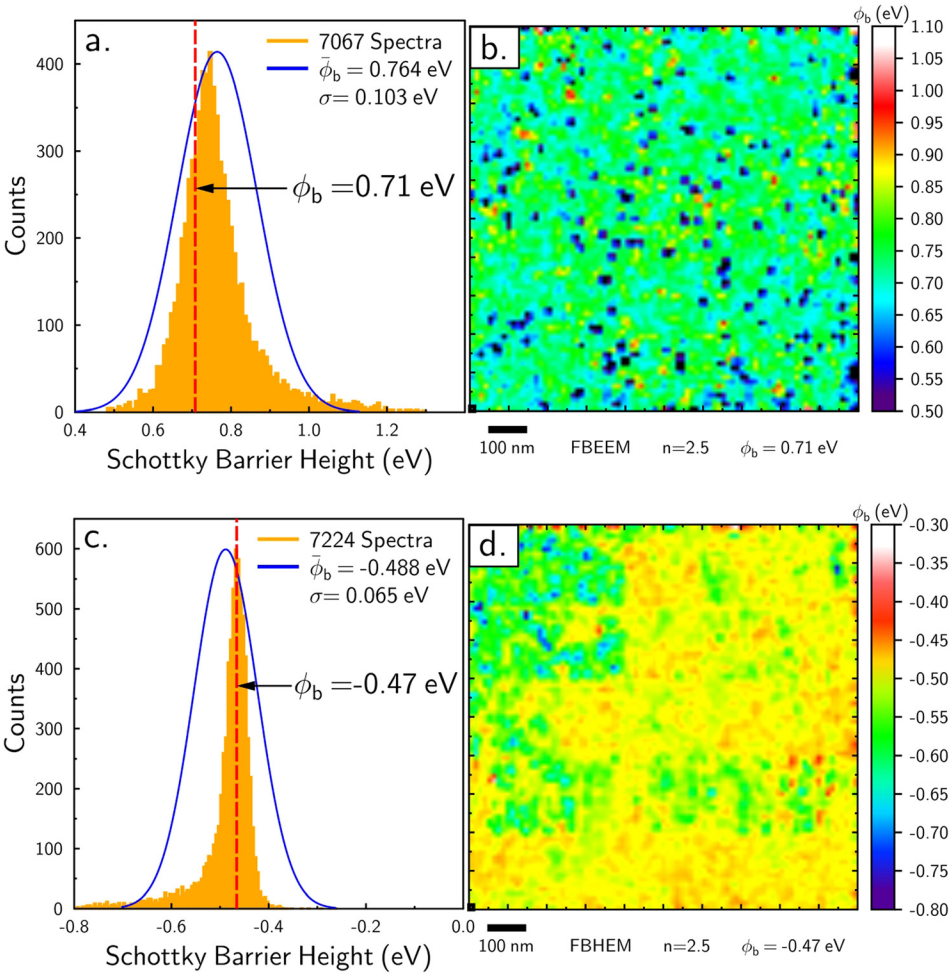

FIG. 5. (a) Histogram of Schottky barrier heights from the 7225 spectra taken on a tungsten *n*-type silicon Schottky junction, the histogram has a standard deviation of 0.103 with an average R^2 value of 0.93. (b) Spatial map of the tungsten to *n*-type silicon Schottky junction in (a). (c) Histogram of Schottky barrier heights from the 7225 spectra taken on a tungsten *p*-type silicon Schottky junction, the histogram has a standard deviation of 0.065 with an average R^2 value of 0.96. (d) Spatial map of *p*-type silicon Schottky junction in (c).

Fig. 3(a). The scatter plot of R^2 vs. Schottky barrier height for all of the 7225 spectra is displayed in Fig. 6(a). The vertical dotted green line is the average R^2 value and the horizontal dotted purple line is the mean Schottky barrier of the distribution. The majority of fits lies close to the intersection of the two lines with a trend to a high R^2 value across all Schottky barrier heights. The spatial map of the barrier heights is displayed in Fig. 5(b). The spatial map shows the variations of the Schottky barrier height at the interface range between 0.65 eV and 0.75 eV and the fluctuations in the barrier height appear to group together. All areas in black are localized spots (~2–4 spectra or 20 nm^2) where no fit was obtained. In addition, there are a few local regions (~2–4 spectra or 20 nm^2) which have a higher Schottky barrier, these points are displayed in red.

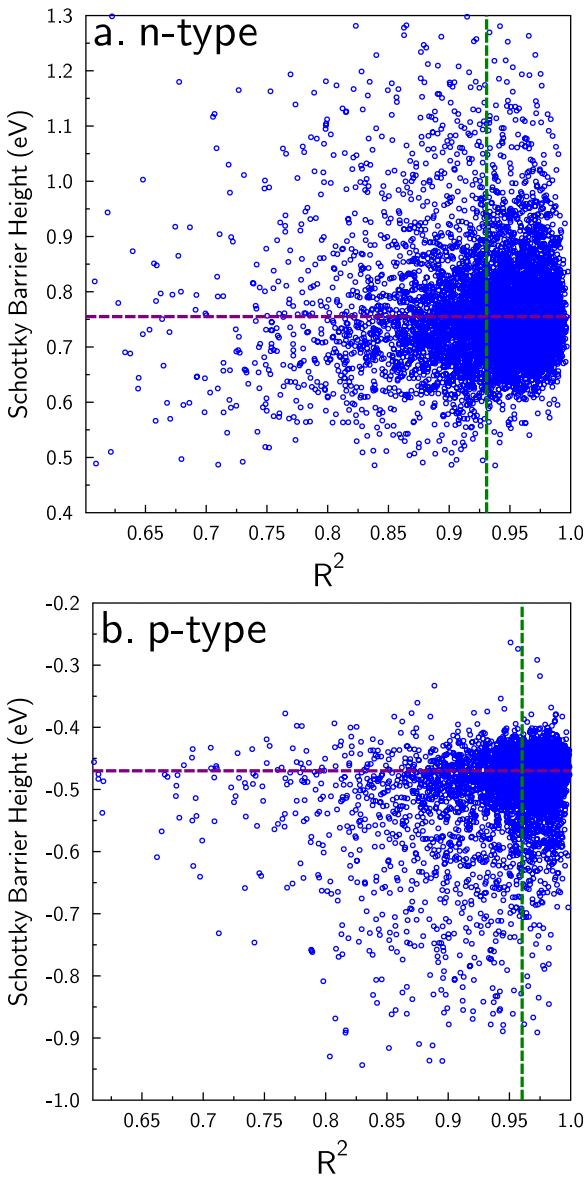

FIG. 6. (a) Scatter plot of R^2 value versus Schottky barrier height for the *n*-type sample. Green dotted line is the average R^2 value and the purple line the mean of the Schottky barrier histogram. (b) Scatter plot of R^2 value versus Schottky barrier height for *p*-type sample. Green dotted line is the average R^2 value and the purple line the mean of the Schottky barrier histogram.

For the *p*-type silicon substrate, a histogram of the barrier heights is displayed in Fig. 5(c). The histogram plots the Schottky barrier height of all of the spectra (99.999%) that could be fit with an average R^2 value of 0.96. The average Schottky barrier and standard deviation of the distribution are utilized to draw a Gaussian as a line over the histogram. The dotted vertical line is the Schottky barrier height determined from the fit to the average spectra, displayed in Fig. 3(c). The scatter plot of R^2 vs. Schottky barrier height for all of the 7225 spectra is displayed in Fig. 6(b). The vertical dotted green line is the average R^2 value and the horizontal dotted purple line is the average Schottky barrier of the distribution. The majority of fits lies close to the intersection of the two lines with a trend to a high R^2 value across all Schottky barrier heights. The spatial map of the barrier heights is displayed in Fig. 5(d). The spatial map shows the variations of the Schottky barrier height at the interface which ranges between −0.45 eV and −0.50 eV and similar to the *n*-type map, the *p*-type map shows the fluctuations in the barrier height appear to group together. All areas in white are localized spots (~2–4 spectra or 20 nm^2) where no fit was obtained. In addition, there are a few local regions (~2–4 spectra or 20 nm^2) which have a higher Schottky barrier, these points are in blue.

IV. DISCUSSION

The interface of tungsten to silicon has been previously studied and has been shown to typically form a silicide with varying stoichiometries depending on deposition conditions.[43,44] In this work, annealing of the sample was intentionally not performed and the BEEM measurements were performed within 24 h to study the as deposited interface. The TEM-EDX and RBS results confirmed that there is a diffusion of tungsten into the silicon lattice and a thin interfacial tungsten silicide less than 5 nm thick is formed. The TEM and RBS both show that there is a layer of gold, a layer of tungsten and gold alloy, and a layer of tungsten. There is no gold present at the silicon to tungsten interface. At the tungsten to silicon interface, the TEM-EDX identifies the presence of tungsten, silicon, and a small amount of oxygen. The hydrofluoric acid etching process removes the native oxide from the surface. However, this small amount of oxygen may be introduced during the deposition from impurities in source material or deposition chamber. A full layer of silicon oxide is not present. This low concentration of oxygen is not seen in the RBS.

The fits to the averaged spectra and the individual spectra were performed using the power law BEEM model.[16] The two most common fitting exponents n are, $n = 2$ Bell and Kaiser (BK), and $n = 5/2$ (PL), where the PL exponent includes the effects of quantum mechanical tunnelling and results in a lower Schottky barrier height.[45] The sum of the absolute value of the *n*-type and *p*-type Schottky barriers for the average BEEM and BHEM spectra equals 1.18 eV using the PL fitting exponent and 1.24 eV using the BK exponent. The bandgap of silicon at 80 K is 1.1669 eV and the PL exponent gives the best agreement with the band gap and is utilized in this study.[46] The power law BEEM

model assumes that measurements are taken at zero temperature. Thermal energy broadening from the measurements being taken at 80 K results in the deviation from the linear behavior and a small amount of transmission below the Schottky barrier, which gets amplified in the linearized spectrum in Fig. 4.

As indicated previously, a non-epitaxial interface will have an inhomogeneous Schottky barrier, which can be accounted for fluctuations in the interface dipoles due to variations in the bonding at the interface.[8] This Schottky barrier energy distribution should be symmetric and the fit to the averaged spectra is expected to be equal to or lower than the mean of the distribution. As the width of the distribution widens, the spectra averaging and fitting process will favor the lower thresholds in the average spectra as it is designed to pick out the first onset in BEEM current. This effect will produce a fit to the average spectra lower than the mean of the distribution, being more pronounced with a wider Schottky barrier distribution. Both the *n*-type and *p*-type diodes show that the Schottky barrier height from the fit to the averaged spectra is shifted to lower energies by less than one standard deviation from the mean of the histogram.

The Schottky barrier histograms for both *n*-type and *p*-type silicon show a slight asymmetric energy distribution to higher energies as seen in Figs. 5(a) and 5(c). The asymmetry in the distribution may arise from stoichiometric fluctuations in the tungsten silicide (i.e., W_xSi_y), where different stoichiometries should result in different Schottky barrier heights. Along with the asymmetry, there are localized spots ($\sim$2–4 spectra or 20 nm^2) which have a Schottky barrier height several standard deviations above the mean, and lie outside the Gaussian envelope. These outliers are attributed to defects or foreign species, such as oxygen forming a local oxide complex. The band offset of a thermally grown SiO_2 film is 3.3 eV as measured with BEEM.[47] However, a thin native oxide cluster would most likely have a lower band offset depending on its stoichiometry, size, and thickness.

The scatter plots show that the distribution of R^2 values as a function of Schottky barrier is focused on the intersection of the average of both values. In addition, a large faction of fits have a high R^2 value which cover the full range of observed Schottky barrier heights. This provides confidence that the higher barrier heights observed are real and result from structure at the interface, which is better visualized in the spatial maps. The Schottky barrier maps for both *n*-type and *p*-type silicon show the spatial distribution of the barrier height. The majority of the area has Schottky barrier heights near the mean of the distribution. In this energy range, the spatial regions of similar barrier heights appear to be grouped together. This intermixing of slightly different Schottky barrier heights is attributed to compositional fluctuations in the tungsten silicide as previously mentioned. For the *n*-type map, there are also individual points which have higher Schottky barrier heights and displayed in red. These points are localized to an area of $\sim$20 nm^2 giving evidence that they are due to some local foreign species or oxide, as mentioned previously. These localized spots are consistent with the small amount of oxygen present in the TEM-EDX measurements. In addition, several locations are black which are of similar size, and there are locations where the individual spectra could not be fit. These spots could be due to a foreign material with a band offset above 2.0 eV or interfacial defect causing elastic scattering. Similar features are seen in the *p*-type map, points where the Schottky barrier is higher ($\sim$ 20 nm^2) are displayed in blue, while points in white were not able to be fit. The structural cause of these localized electronic defects can be much smaller than what is imaged since even atomic structural perturbations can have a much larger spatial effect on the charge distribution at the interface.

V. CONCLUSIONS

The Schottky barrier of the W/Si(001) diode has been studied using BEEM and BHEM. Utilizing both *n*-type and *p*-type silicon, the band gap of silicon was extracted using the simplified BEEM model based on the PL fitting exponent. The material stack was examined using TEM, EDX, and RBS, where a thin tungsten silicide was found to form at the interface. Schottky barrier histograms show a Gaussian distribution of the Schottky barrier consistent with an interface dipole model as well as deviations attributed to compositional fluctuations, defects, and foreign materials. Spatial maps show the uniformity of the Schottky barrier and demonstrate the ability to image the nanoscale electronic structure and defects of a buried interface with BEEM.

ACKNOWLEDGMENTS

The authors acknowledge the support of the Semiconductor Research Corporation, Center for advanced Interconnect Science and Technology, and the National Science Foundation Grant No. DMR-1308102, and SEMATECH.

[1]S. K. Cheung and N. W. Cheung, Appl. Phys. Lett. **49**, 85 (1986).
[2]T. Arizumi and M. Hirose, Jpn. J. Appl. Phys. Part 1 **8**, 749 (1969).
[3]B. E. Coss, P. Sivasubramani, B. Brennan, P. Majhi, R. M. Wallace, and J. Kim, J. Vac. Sci. Technol., B **31**, 021202 (2013).
[4]S. Smith, K. Aouadi, J. Collins, E. van der Vegt, M.-T. Basso, M. Juhel, and S. Pokrant, Microelectron. J. **82**, 261 (2005).
[5]S. Haimsona, Y. Shacham-Diamand, D. Horvitz, and A. Rozenblat, Microelectron. Eng. **92**, 134 (2012).
[6]F. Papadatos, K. Wong, V. Arunachalam, C. H. Shin, Z. Li, M. Chudzik, W.-H. Lee, and A. Xing, Microelectron. Eng. **92**, 123 (2012).
[7]M. Tsai, H. Chao, L. Ephrath, B. Crowder, A. Cramer, R. Bennett, C. Lucchese, and M. Wordeman, J. Electrochem. Soc. **128**, 2207 (1981).
[8]R. T. Tung, Phys. Rev. B **45**, 13509 (1992).
[9]N. Mott, Proc. R. Soc. London, Ser. A **171**, 27 (1939).
[10]C. Detavernier, R. L. Van Meirhaeghe, R. Donaton, K. Maex, and F. Cardon, J. Appl. Phys. **84**, 3226 (1998).
[11]G. M. Vanalme, L. Goubert, R. L. V. Meirhaeghe, F. Cardon, and P. Van Daele, Semicond. Sci. Technol. **14**, 871 (1999).
[12]P. N. First, J. A. Stroscio, R. A. Dragoset, D. T. Pierce, and R. J. Celotta, Phys. Rev. Lett. **63**, 1416 (1989).
[13]A. M. Cowley and S. M. Sze, J. Appl. Phys. **36**, 3212 (1965).
[14]J. Y. Duboz, P. A. Badoz, F. Arnaud d'Avitaya, and E. Rosencher, Phys. Rev. B **40**, 10607 (1989).
[15]R. T. Tung, J. Vac. Sci. Technol., B **2**, 465 (1984).
[16]L. D. Bell and W. J. Kaiser, Phys. Rev. Lett. **61**, 2368 (1988).
[17]M. K. Weilmeier, W. H. Rippard, and R. A. Buhrman, Phys. Rev. B **59**, R2521 (1999).
[18]M. K. Weilmeier, W. H. Rippard, and R. A. Buhrman, Phys. Rev. B **61**, 7161 (2000).
[19]W. J. Kaiser, M. H. Hecht, R. W. Fathauer, L. D. Bell, E. Y. Lee, and L. C. Davis, Phys. Rev. B **44**, 6546 (1991).

[20]H. Sirringhaus, T. Meyer, E. Y. Lee, and H. von Känel, Phys. Rev. B **53**, 15944 (1996).
[21]C. A. Bobisch, A. Bannani, Y. M. Koroteev, G. Bihlmayer, E. V. Chulkov, and R. Moller, Phys. Rev. Lett. **102**, 136807 (2009).
[22]C. A. Ventrice, Jr., V. P. LaBella, G. Ramaswamy, H. P. Yu, and L. J. Schowalter, Phys. Rev. B **53**, 3952 (1996).
[23]I. Sitnitsky, J. J. Garramone, J. Abel, P. Xu, S. D. Barber, M. L. Ackerman, J. K. Schoelz, P. M. Thibado, and V. P. LaBella, J. Vac. Sci. Technol., B **30**, 04E110 (2012).
[24]J. J. Garramone, J. R. Abel, I. L. Sitnitsky, L. Zhao, I. Appelbaum, and V. P. LaBella, Appl. Phys. Lett. **96**, 062105 (2010).
[25]H. J. Im, B. Kaczer, J. P. Pelz, and W. J. Choyke, Appl. Phys. Lett. **72**, 839 (1998).
[26]C. Tivarus, J. P. Pelz, M. K. Hudait, and S. A. Ringel, Phys. Rev. Lett. **94**, 206803 (2005).
[27]T. Banerjee, E. Haq, M. Siekman, J. Lodder, and R. Jansen, IEEE Trans. Magn. **41**, 2642 (2005).
[28]J. J. Garramone, J. R. Abel, S. Barraza-Lopez, and V. P. LaBella, Appl. Phys. Lett. **100**, 252102 (2012).
[29]J. J. Garramone, J. R. Abel, I. L. Sitnitsky, and V. P. LaBella, J. Vac. Sci. Technol., A **28**, 643 (2010).
[30]J. J. Garramone, J. R. Abel, I. L. Sitnitsky, R. L. Moore, and V. P. LaBella, J. Vac. Sci. Technol. B **27**, 2044 (2009).
[31]A. J. Stollenwerk, M. R. Krause, D. H. Idell, R. Moore, and V. P. LaBella, J. Vac. Sci. Technol., B **24**, 2009 (2006).
[32]A. Stollenwerk, M. Krause, R. Moore, and V. P. LaBella, J. Vac. Sci. Technol., A **24**, 1610 (2006).
[33]H. L. Qin, K. E. J. Goh, M. Bosman, K. L. Pey, and C. Troadec, J. Appl. Phys. **111**, 013701 (2012).
[34]S. Forment, R. L. Van Meirhaeghe, A. D. Vrieze, K. Strubbe, and W. P. Gomes, Semicond. Sci. Technol. **16**, 975 (2001).
[35]M. Prietsch, Phys. Rep. **253**, 163 (1995).
[36]M. Prietsch and R. Ludeke, Phys. Rev. Lett. **66**, 2511 (1991).
[37]T. Meyer and H. von Knel, Phys. Rev. Lett. **78**, 3133 (1997).
[38]H. Palm, M. Arbes, and M. Schulz, Phys. Rev. Lett. **71**, 2224 (1993).
[39]A. E. Fowell, R. H. Williams, B. E. Richardson, A. A. Cafolla, D. I. Westwood, and D. A. Woolf, J. Vac. Sci. Technol., B **9**, 581 (1991).
[40]A. E. Fowell, R. H. Williams, B. E. Richardson, and T. H. Shen, Semicond. Sci. Technol. **5**, 348 (1990).
[41]A. Olbrich, J. Vancea, F. Kreupl, and H. Hoffmann, J. Appl. Phys. **83**, 358 (1998).
[42]M. Krause, A. Stollenwerk, C. Awo-Affouda, B. Maclean, and V. P. LaBella, J. Vac. Sci. Technol., B **23**, 1684 (2005).
[43]F. M. d'Heurle, C. S. Petersson, and M. Y. Tsai, J. Appl. Phys. **51**, 5976 (1980).
[44]S. Itoh, J. Phys.: Condens. Matter **2**, 3747 (1990).
[45]R. Ludeke and M. Prietsch, J. Vac. Sci. Technol., A **9**, 885 (1991).
[46]W. Bludau, A. Onton, and W. Heinke, J. Appl. Phys. **45**, 1846 (1974).
[47]B. Kaczer, Z. Meng, and J. P. Pelz, Phys. Rev. Lett. **77**, 91 (1996).